frontiers in Environmental Science

ORIGINAL RESEARCH
published: 30 June 2020
doi: 10.3389/fenvs.2020.00091

Single- and Multi-Element Quantification and Characterization of TiO_2 Nanoparticles Released From Outdoor Stains and Paints

*Agil Azimzada[1,2], Jeffrey M. Farner[2], Ibrahim Jreije[1], Madjid Hadioui[1], Carolyn Liu-Kang[1], Nathalie Tufenkji[2], Phil Shaw[3] and Kevin J. Wilkinson[1]**

[1] Department of Chemistry, University of Montreal, Montreal, QC, Canada, [2] Department of Chemical Engineering, McGill University, Montreal, QC, Canada, [3] Nu Instruments Ltd, Wrexham, United Kingdom

With growing applications of TiO_2 nanoparticles (NPs) in outdoor surface coatings, notably in paints and stains, their release into the environment is inevitable. While NP release has potential ecotoxicological risk, reliable risk assessments are often complicated by the near absence of analytical data on release rates under natural weathering scenarios, and the lack of a chemical characterization of the NPs following their release. This work measured NPs released from painted and stained surfaces and characterized them by size and composition using magnetic sector single particle inductively coupled plasma mass spectrometry (SP-ICP-MS) and SP-ICP-time-of-flight-MS (SP-ICP-TOF-MS). Two *in situ* experimental plans were examined in which natural precipitation interacted with nano-enhanced surfaces to varying degrees during the fall and winter. Weathering data showed that longer contact times of the precipitation (snow and rain) resulted in greater NP release. Although the stained surfaces had far fewer NPs per unit area, they lost a much higher fraction of their NP load (max 6% leached, as opposed to $<10^{-4\%}$ in paints), over similar exposure times. NP release was particularly enhanced for conditions of frequent rainfall and spring snow melt (i.e., slushy snow). SP-ICP-TOF-MS measurements on the Ti NPs indicated that they were often associated with a secondary metal in both the liquid paint (Al was detected in ∼20% of the Ti NPs; Zr in about ∼1% of the NP) and the liquid stain (Fe was detected in ∼7%, Si in ∼8% and Al in ∼3% of the Ti NPs). In contrast, for the vast majority of Ti NPs being leached out of the painted/stained surfaces, only Ti was detected. Metal interactions in the paint were explained by binding of the TiO_2 within a complex paint matrix; while in the stain, TiO_2 NPs were hypothesized to be found in heteroagglomerates, potentially with aluminosilicates (Fe, Si, and Al). In rain and snow, Ti was the only element detected in about half of the Ti NPs; in the other half, Ti often co-occurred with Fe, Si and Al. The results indicate that single element, likely anthropogenic, Ti NPs are already prevalent in the natural precipitation and that NP release from surface coatings will further increase their presence in the environment.

Keywords: nanomaterial, release, paint, stain, titania, SP-ICP-TOF-MS, weathering, environment

OPEN ACCESS

Edited by:
Vera I. Slaveykova, Université de Genève, Switzerland

Reviewed by:
Francisco Laborda, University of Zaragoza, Spain
Mohammed Baalousha, University of South Carolina, United States

****Correspondence:***
Kevin J. Wilkinson
kj.wilkinson@umontreal.ca

Specialty section:
This article was submitted to Biogeochemical Dynamics, a section of the journal Frontiers in Environmental Science

Received: *30 March 2020*
Accepted: *03 June 2020*
Published: *30 June 2020*

Citation:
Azimzada A, Farner JM, Jreije I, Hadioui M, Liu-Kang C, Tufenkji N, Shaw P and Wilkinson KJ (2020) Single- and Multi-Element Quantification and Characterization of TiO_2 Nanoparticles Released From Outdoor Stains and Paints. Front. Environ. Sci. 8:91. doi: 10.3389/fenvs.2020.00091

INTRODUCTION

A rapid increase in the adoption of nanotechnologies across numerous industries has been a major driver in the production and use of engineered nanomaterials (ENMs) (Robichaud et al., 2009; Vance et al., 2015). Paints and stains represent two important applications of ENMs, for which TiO_2 nanoparticles (NPs) are extensively used for improved UV protection and self-cleaning properties (Hincapié et al., 2015; Hischier et al., 2015). The increasing development of nano-enabled coatings will invariably lead to increased environmental release of TiO_2 NPs, prompting questions about their fate and bioavailability (Auffan et al., 2009; Van Broekhuizen et al., 2011; Nowack et al., 2012; Sun et al., 2014; Hischier et al., 2015; Mitrano et al., 2015; Coll et al., 2016).

Although some environmental and health hazards have been associated with TiO_2 NPs (Zhu et al., 2011; Simonin et al., 2017; Farner et al., 2019; Liu et al., 2019), the extent of their release from different outdoor coatings has not been well investigated, especially under variable climatic conditions. The near absence of measured environmental concentrations of TiO_2 (or any other) NPs greatly complicates their risk assessment. Indeed, most laboratory and *in situ* studies on NP release from coatings have been limited to a qualitative or semi-quantitative demonstration of release (e.g., with microscopy) or quantitative measurements based on the total metal content (Kägi et al., 2008; Olabarrieta et al., 2012; Al-Kattan et al., 2013; Zuin et al., 2014; Hincapié et al., 2015; Hischier et al., 2015; Kaegi et al., 2017; Zhang et al., 2017; Clar et al., 2018, 2019) – rather than a specific determination of the NP forms. Using a sensitive, magnetic-sector ICP-MS, we were recently (Azimzada et al., 2020) able to quantify mass and number release rates of TiO_2 NPs from painted surfaces during natural weathering cycles. While that study provided valuable information on real-life NP release quantities and particle size distributions, the data was mainly relevant for surfaces that were likely to retain the incoming snow or rainwater. It showed that the wet surface interaction time (i.e., contact time between the precipitation and the surface) was a critical environmental variable affecting NP release. Nonetheless, the study did not look at other outdoor surfaces, notably façades, or other nano-enhanced surfaces, such as stains. Furthermore, a major difficulty was the ability to distinguish Ti-rich natural colloids from TiO_2 NPs (Wagner et al., 2014; del Real et al., 2018).

Both exposure conditions and the nature of the coating will influence NP leaching and their interactions with other chemical constituent(s). For example, paint-released NPs have been shown to be embedded in their original paint matrix (Kaegi et al., 2010; Al-Kattan et al., 2014), which may result in them acting as a vector for the release and transport of other potentially toxic chemicals. Furthermore, while metal-based, manufactured NPs are often assumed to be composed of single elements or metal oxides (Loosli et al., 2019), only limited datasets are available with respect to their actual chemical identities, including metallic impurities, surface coatings, etc. While quantitative measurements of NP exposure concentrations are necessary for risk determinations, characterization of the released NP and their associations with other elements is necessary in order to define chemical hazard.

ICP-MS based techniques are well-suited for NP quantification as they are extremely sensitive, high-throughput and analyte-specific techniques that can quantify metal-based NPs and determine their size distributions on a single particle basis (Montaño et al., 2016; Azimzada et al., 2017; Gondikas et al., 2018; Meermann and Nischwitz, 2018). By analyzing the transient ICP-MS signal, NPs are identified as high-intensity spikes against a continuous background signal that is attributed to dissolved metals and background interferences (Degueldre et al., 2006; Tharaud et al., 2017). While single-particle ICP-MS (SP-ICP-MS) provides targeted single-element analysis of the NPs, SP-ICP-time-of-flight-MS (SP-ICP-TOF-MS) is able to simultaneously identify and quantify a full spectrum of elements in single particles (Hendriks et al., 2017, 2018; Praetorius et al., 2017). Nonetheless, due to the nature of the technology and the multiplicity of analytes in a single particle, SP-ICP-TOF-MS generally has higher size detection limits than SP-ICP-MS (Meermann and Nischwitz, 2018; Mozhayeva and Engelhard, 2020). For example, for Ti-containing NPs in surface waters, minimum detectable sizes of $<$20 nm have been determined using a high-resolution SP-ICP-MS (Hadioui et al., 2019; Azimzada et al., 2020), whereas size detection limits are typically above 60 nm when using SP-ICP-TOF-MS (Gondikas et al., 2018; Mozhayeva and Engelhard, 2020).

Given the above knowledge gaps, this study was designed to analyze TiO_2 NP release from two nano-enhanced surfaces under different weathering scenarios. Technical challenges were addressed by using recent improvements (Hadioui et al., 2019) in sensitivity and data treatment for both SP-ICP-MS and SP-ICP-TOF-MS. The specific objectives were: (i) to quantify and characterize TiO_2 NP release from a paint and a stain under natural weathering scenarios, and (ii) to distinguish TiO_2 NPs from the high quantity of colloidal Ti particles found in natural precipitation.

MATERIALS AND METHODS

Weathering Panels

Untreated oak slats were cut to obtain panels that were 0.64 cm thick, 6.4 cm wide and 8.4 cm long. They were subsequently painted (Behr Premium Plus Ultra Exterior Satin Enamel Ultra-Pure White paint) or stained (SICO exterior semi-transparent wood stain) with products that were advertised for their Nanoguard Technology and/or nano-sized pigments. The paint was uniformly distributed by applying 15 mL per side of each panel using a film applicator (Bird Film Applicator, Inc., Washington, United States) (Azimzada et al., 2020) with removal of the excess paint. Due to its lower viscosity, 5 mL of stain was applied per side using a paintbrush. Panel surfaces were coated twice on each side and at least two days was allowed for drying between each coat. The final dry paint or stain loadings were similar among panels for each coating type: 400 $\pm$ 40 g-paint

m^{-2} (or 4.4 g-paint per panel) and 36 ± 3 g-stain m^{-2} (or 0.4 g-stain per panel).

Natural Weathering Setups

The outdoor weathering setup consisted of two experimental designs – namely, vertical and slanted designs – that simulated two environmentally relevant weathering scenarios. The vertical design was designed to be more representative of a scenario where a surface is weathered by stationary water or snow accumulation (e.g., puddle or snow on a deck), whereas the slanted design was designed to represent the weathering of outdoor façades where precipitation does not accumulate on the surface. In the ***vertical design***, painted/stained panels were vertically positioned in pre-weighed, wide-mouth polypropylene containers (500 mL, Fisher Scientific) (**Figure 1A**). Every 2,3 weeks, panels were removed from the containers, and then placed outside in a new (empty) container. In the ***slanted design***, two polypropylene containers were fixed on top of each other and separated by a polypropylene mesh (**Figure 1B**). The mesh supported the panel, which was fixed in a slanted position in the top section. Rain came into contact with the panel and then flowed into the bottom container (the leachate collector), whereas snow had a tendency to sometimes collect on the surface of the panel. For each timepoint, the bottom container was removed, capped and replaced by another pre-labeled, pre-weighed and pre-cleaned container.

Due to the ubiquitous presence of nano- and micron-sized particles in the precipitation (Hochella et al., 2019; Rahim et al., 2019; Azimzada et al., 2020), one critical challenge in the experiments was to quantitatively distinguish NPs that were leached out of painted surfaces from background NPs in the natural precipitation (Wagner et al., 2014). Control experiments were thus critical to accurately determining NP release, with sufficient replication at each timepoint (n = 4). The use of untreated wooden panels was ruled out based on the preliminary observations that they rapidly disintegrated when subjected to natural weathering. Thus, for both designs, controls consisted of empty containers that were placed alongside exposure samples in order to collect the incoming precipitation (Azimzada et al., 2020). Containers were randomly placed in plastic bins, which protected them from tipping over by minimizing the impact of side winds. Bins were then placed outdoors on a 7th floor roof (Pavillon Roger-Gaudry, University of Montreal, Montreal, Canada). Samples were left undisturbed, unless they were buried by snow, in which case, excess snow was carefully scraped off the top of the containers (Azimzada et al., 2020). Fall weathering experiments started at the beginning of October 2018 and lasted for 11 weeks, while winter weathering experiments extended from late January (2019) until early April for a duration of 12 weeks. All exposure and control samples included 4 replicates. For the last two timepoints of the fall weathering series, the slanted samples tipped over and thus, the results for those timepoints are not available.

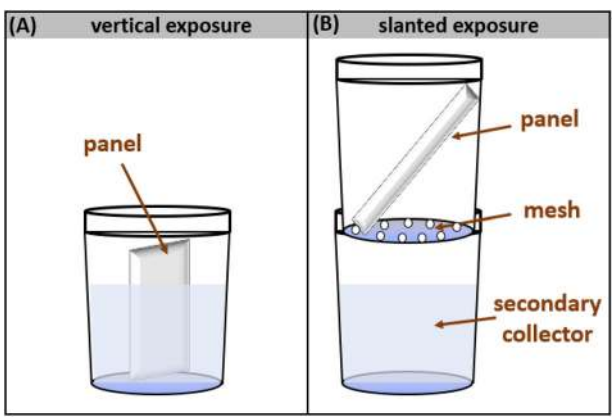

FIGURE 1 | Experimental setups for two weathering scenarios: **(A)** vertical exposure – consisting of a painted/stained panel vertically positioned in a polypropylene container, **(B)** slanted exposure – made up of two containers stacked on top of each other and separated by a polypropylene mesh, where the top container contains a painted/stained panel fixed in a slanted position. The vertical exposure is more representative of a surface in more sustained contact with precipitation whereas the slanted exposure is designed to be more representative of the weathering of an outdoor façade. Panels did not extend out of the containers, but rather they were custom cut to fit in the containers, while leaving an overhead space equivalent to 15% of the container height.

Indoor Weathering

To characterize surface-leached NPs using SP-ICP-TOF-MS, painted and stained (each with four replicates) panels were placed vertically into pre-weighed polypropylene containers, which were filled with 380 mL of Milli-Q water (i.e., panels fully immersed). Surfaces were then subjected to accelerated aging under freeze-thaw conditions, which involved successive cycles of 24 h freezing and 24 h thawing over 3 weeks (Azimzada et al., 2020). Following the freeze-thaw cycles, leachates were collected and prepared for SP-ICP-TOF-MS analysis.

Sample Preparation for SP-ICP-MS/SP-ICP-TOF-MS

At each timepoint, samples (exposure and controls) were brought inside the lab, left to melt and then gently mixed. The samples were then weighed and placed in a sonicator bath for 30 minutes (Branson Ultrasonic Cleaner, 5510R-DTH Model, 135 W, 42 kHZ ± 6%). Eight (8) to 10 mL of the samples were filtered (0.45 μm cut-off) through a 33 mm diameter PVDF (Polyvinylidene fluoride) syringe filter (Sigma-Aldrich) that had been pre-rinsed with 12 mL Milli-Q water and 6 mL of sample (Azimzada et al., 2020). The filtration step is designed to protect the nebulizers by avoiding build-up and blockage, while being large enough to minimize exclusion of the NPs. While pre-rinsing the filter with sample minimizes adsorptive losses, the 0.45 μm cutoff is nonetheless operationally defined- particle losses would lead to an underestimation of particle numbers.

SP-ICP-MS Analysis and Data Acquisition

SP-ICP-MS measurements were performed on a magnetic sector ICP-MS (AttoM ES, Nu Instruments, United Kingdom), at low

resolution (300), using single ion acquisition in fast-scan mode (Shaw and Donard, 2016). To further enhance the sensitivity, the ICP-MS used a desolvator (Aridus II, Teledyne Cetac Technologies), which utilized a PFA (perfluoroalkoxy) micro-flow nebulizer (self-aspiration rate of 200 μL min^{-1} at 1 L min^{-1} of Ar) (Fréchette-Viens et al., 2019; Hadioui et al., 2019). Optimized membrane sweep gas (argon) flow rates typically ranged between 3–7 L min^{-1}, while the nebulizer gas (argon) flow was between 0.7–1.0 L min^{-1}. In accordance with previously optimized strategies (Hadioui et al., 2019) to lower the size detection limits (SDL) 49Ti was chosen for analysis. With an acquisition time of 50 s per sample and an optimized dwell time of 50 μs (Hadioui et al., 2019), ca. 10 (Hischier et al., 2015) datapoints were obtained per replicate. Sensitivity calibrations for 49Ti were based on ionic standards (High Purity Standards) and transport efficiency (TE) measurements were performed using a suspension of ultra-uniform 30 nm Au NPs (NanoComposix, AUXU30-1M) that were previously validated using a second standard reference material (60 nm Au NPs, NIST8013) (Hadioui et al., 2019). Standards for TE measurements were prepared daily at 50 ng L^{-1}. TE values ranged between 13–15%, corresponding to an actual sample injection into the plasma of 0.45–0.55 μL s^{-1}. Filtered samples were diluted up to 10× to ensure that the incidences of concurrent peaks were minimized (less than 10,000 events or 1% of total datapoints), while ensuring a statistically significant number of NPs (>500 events). Matrix effects were not observed (Azimzada et al., 2020).

SP-ICP-TOF-MS Analysis and Data Acquisition

SP-ICP-TOF-MS measurements were performed on a time-of-flight ICP-MS (Nu Vitesse, Nu Instruments, United Kingdom), using a segmented reaction cell with ca. 4–6 cm^3 min^{-1} of He and ca. 4 cm^3 min^{-1} of H_2 gas introduced to eliminate argon and nitrogen-based interferences. This method improved the sensitivity of the technique by allowing the higher abundance isotopes of elements like Si, K, Ca, Cr, Fe, and Se to be monitored without interference. A near full range of time of flight mass spectra (23–238 amu) were acquired every 25.5 μs, and three acquisitions were combined before electronics noise was subtracted and isotope signals were integrated over their defined mass positions to produce individually stored measurements for Na to U, every 76 μs. Data were acquired for a total sampling time of about 30 s, for the most concentrated samples, to a maximum of 2 min for dilute samples. Mass spectra were acquired continuously, in an uninterrupted manner and without loss of data. Sensitivity was further improved by using an Aridus II desolvator as above, with similar parameters as the magnetic sector instrument. TE was determined using the particle size method (Pace et al., 2011) by measuring the instrument sensitivity (counts s^{-1} ng L^{-1}) for ionic gold standards and mass sensitivity (counts ng^{-1}) for a highly monodisperse Au NP standard (known size and density). This led to TE values ranging between 10–15%. An ultra-uniform NP standard of 30 nm (NanoComposix, AUXU30-1M) was used to calculate TE, while 60 nm Au NP (NanoComposix) and 40 nm Ag (NanoComposix) standards were used for validation of the TE values. A multi-element standard (SPEX CertiPrep) containing all metals was used for ionic sensitivity determinations.

SP-ICP-MS/SP-ICP-TOF-MS Data Processing

SP-ICP-MS data were analyzed using NuQuant software version 2.2 (Nu Instruments, United Kingdom), based on the methodology described in Hadioui et al. (2019) and Shaw and Donard (2016). In summary, the data analysis algorithm used data smoothing to reduce baseline fluctuations; created rolling search windows where it searched for NP peaks based on maximum intensities; and calculated local backgrounds for each peak based on data preceding the pre-inflection points. For each detected NP, the local background was subtracted from the integrated raw data, while the average of local peak backgrounds was used to calculate dissolved metal contents.

For SP-ICP-TOF-MS data, a modified version of NuQuant software (NuQuant Vitesse prototype, Nu Instruments, United Kingdom) was used, where the algorithm searched for a target isotope, here 48Ti, using similar smoothing and peak detection parameters as in the single-particle analysis. The start and end timestamps for each detected particle event were determined and used to identify counts for all isotopes. The full width half maximum (FWHM) values, along with the standard deviation of the background (for each isotope) were used to estimate the noise threshold, above which particle events were reported. This threshold, typically consisting of 5–7 multiples of the standard deviation of the background, was applied to filter out background artifacts while optimizing the detection of real NP peaks. Elements of interest (especially those with low intensities) were visually checked to ensure that background artifacts were avoided (i.e., very slender or very wide peaks with low intensity).

NP masses (and sizes if density and shape can be assumed) were calculated using calibrated multi-element sensitivities and transport efficiency measurements obtained for the monodisperse Au NPs (Pace et al., 2011). Size calculations for TiO_2 were performed by assuming a spherical particle with a density of 4.23 g cm^{-3}, corresponding to rutile (Azimzada et al., 2020).

Ti Analysis by Quantitative ICP-MS

Given the very low Ti concentrations in the precipitation samples (i.e., ng L^{-1} levels) and dilutions required to reduce acid concentrations prior to ICP-MS analysis, the use of digestion protocols (Gondikas et al., 2014; Loosli et al., 2019) to obtain total Ti was unfortunately not viable here. Ti measurements were nonetheless performed on leachate samples, following filtration over a 0.45-μm PVDF filter and addition of 67–70% HNO_3 (ultratrace grade, BDH Aristar Ultra) in polypropylene tubes to obtain a final acid content of 20% v/v. Samples were left for 16 h at 85 °C in a DigiPREP digestion system (SCP Science) (Azimzada et al., 2020) and

then diluted 5–10× with Milli-Q water to obtain a final HNO_3 content of 2–4% v/v for the ICP-MS analysis. The measured Ti nominally included dissolved Ti as well as any of the sub-0.45-μm particles. Although the addition of concentrated HNO_3 is not sufficient for the complete digestion of the TiO_2 (De la Calle et al., 2016), measurements were performed to provide some additional validation of the single-particle techniques for which particle concentrations are determined from the number of transient peaks, using a non-acidified sample (i.e., greater potential for adsorptive losses). Digested Ti thus represents an operationally defined fraction (Azimzada et al., 2020) that may not capture all of the colloidal Ti in the sample.

RESULTS AND DISCUSSION

Technical Considerations in the SP-ICP-MS and SP-ICP-TOF-MS Measurements

Fewer than three spikes per min were generally observed for a Milli-Q water blank (Fréchette-Viens et al., 2019). By assuming

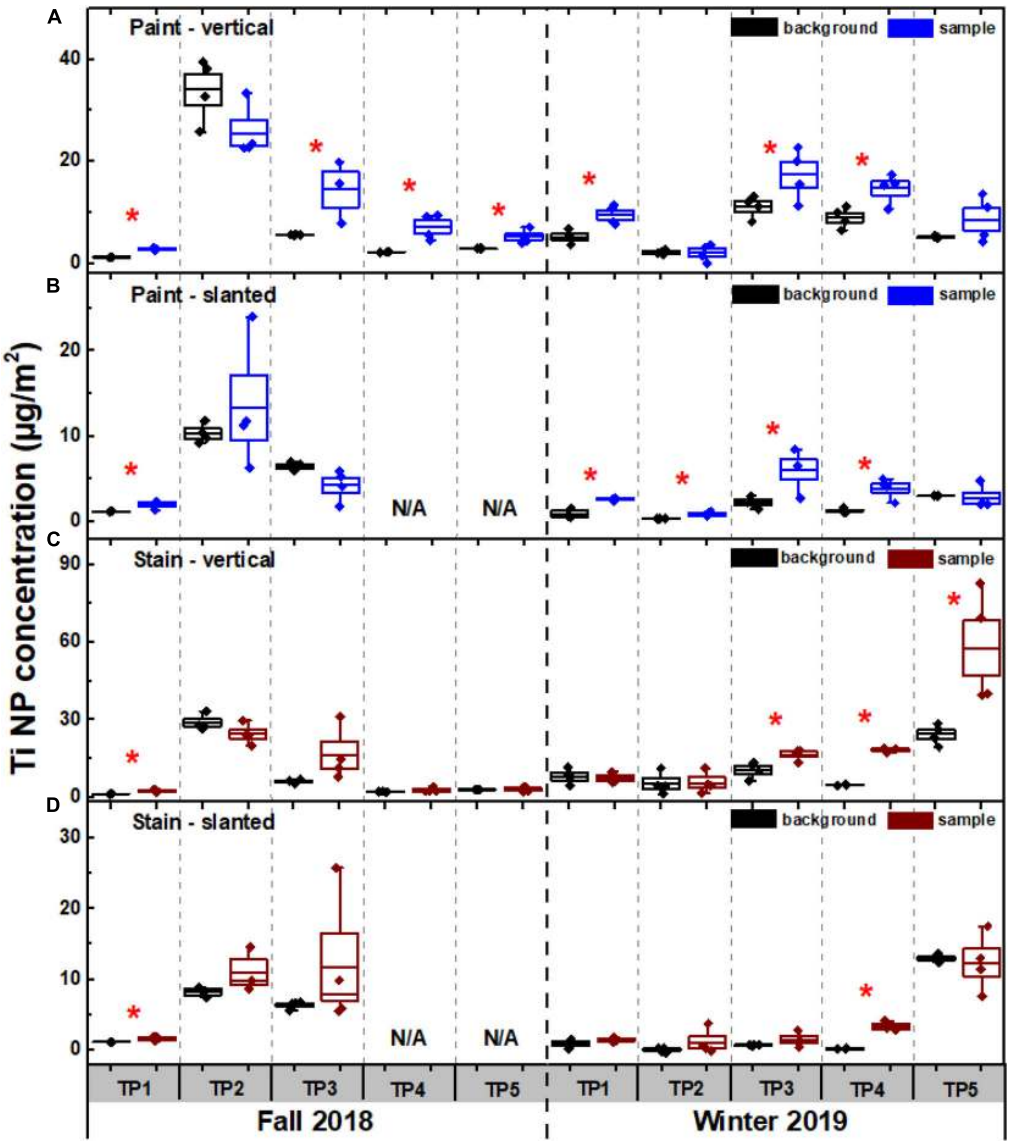

FIGURE 2 | Quantification of Ti containing NPs in the precipitation (i.e. background) and in the precipitation following its contact with **(A,B)** painted and **(C,D)** stained panels. Weathering experiments were conducted using two exposure designs (**Figure 1**), **(A,C)** vertical and **(B,D)** slanted, for painted and stained panels. A red star indicates a significant difference ($N = 4$, student t-test, $p < 0.05$) between the NP content in the background and the NP content in the sample. NP concentrations were normalized by the surface area of the painted/stained panels subjected to weathering. Containers were renewed at each timepoint (TP). Measurements were performed using a magnetic sector ICP-MS in single particle mode. Measured NP content includes particles between the instrumental size detection limit of ∼15 nm and the filtration cut-off (0.45 μm). N/A denotes two samples that were lost.

that the detection of 10 NPs during a 50 s acquisition would be required in order to have sufficient confidence that particles were being detected (Laborda et al., 2019), one can estimate a detection threshold of ca. 360 NP mL^{-1} with a minimum detectable (TiO_2 equivalent) particle size of ∼15 nm (**Supplementary Figure S1A**). The size detection limit compare favorably with those that have generally been determined by SP-ICP-MS [∼60 nm (Gondikas et al., 2014; Lee et al., 2014)]. The SP-TOF-ICP-MS had higher, matrix-sensitive size detection limits, ranging from 30 nm (in Milli-Q water) to 46 nm (in the rain) (i.e., assuming spherical TiO_2 particles, **Supplementary Figure S2**). In that case, minimum detectable particle numbers were kept <1000 mL^{-1} by increasing the acquisition time to 120 s. For both techniques, raw data corresponding to NPs that are close to instrumental size detection limits have been provided in **Supplementary Figures S1B**, **S2B,D,F** for the different matrices. In all cases, NP concentrations in the samples were consistently above 10,000 mL^{-1}, well above the detection limits. While these detection limits are among the lowest in the literature for TiO_2, it is important to note that "nanoparticle" number measurements presented below are necessarily for particles that are larger than the lower size detection limits (e.g., 15 nm by magnetic sector SP-ICP-MS; 34 nm by SP-TOF-ICP-MS) but smaller than the filtration cut-off (i.e., 0.45 μm).

Characterization of TiO_2 NPs in the Paint and Stain

Immediately prior to analysis by SP-ICP-MS, liquid acrylic paint was diluted $2 \times 10^7\times$ in Milli-Q water, while stain was diluted $2 \times 10^5\times$. TiO_2 NPs in the paint were fairly polydisperse with a particle size distribution extending from about 20 nm (just above the size detection limit) to beyond 200 nm (**Supplementary Figure S3A**), with a concentration of $(6.8 \pm 0.1) \times 10^{15}$ NPs kg-paint^{-1}. TiO_2 NPs in the stain were smaller with a majority (>95%) of the particles between 20 and 100 nm (**Supplementary Figure S3B**) and a

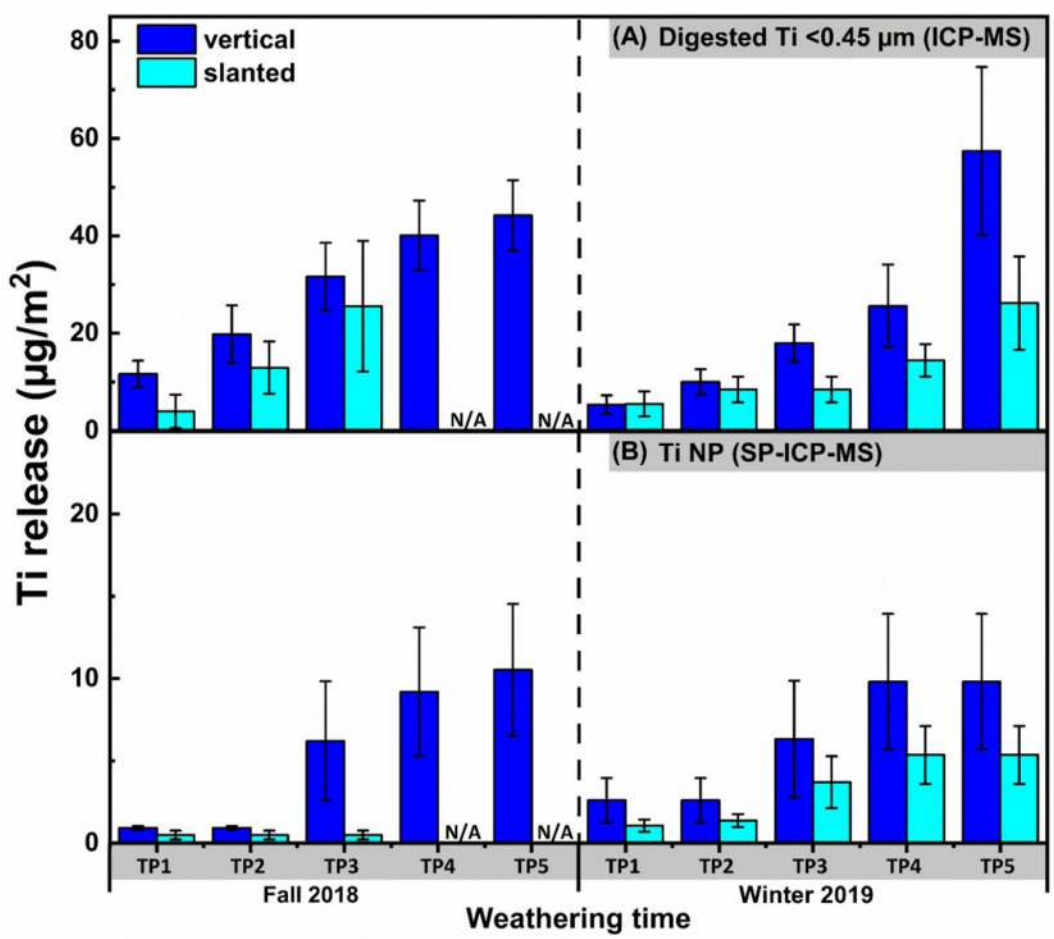

FIGURE 3 | Cumulative concentrations of sub-0.45-μm Ti determined by **(A)** ICP-MS on acidified samples and **(B)** SP-ICP-MS, obtained by integration of the NP peaks. Ti was measured following its release from the **painted** surfaces in vertical and slanted exposure modes (N = 4 for each condition). Release was normalized by the surface area of the painted panels that were subject to weathering and corrected for the pre-existing natural background in the precipitation. Measurements were performed using a magnetic sector ICP-MS. N/A denotes two samples that were lost.

concentration of $(2.9 \pm 0.4) \times 10^{13}$ NPs kg-stain^{-1}. Number-based average particle sizes corresponded to 131 ± 53 nm in the liquid paint and 42 ± 24 nm in the stain, where standard deviations reflected polydispersities, rather than errors determined on repeated measurements (typically ∼3 nm). Particle concentrations corresponded to about 5% w/w in the paint and 0.001% w/w NP in the stain.

Release of NPs From Painted and Stained Surfaces

In spite of precautions that included the use of four replicates for samples and controls; their randomization in the protective bins and the lowering of detection limits of the SP-ICP-MS technique; there were still cases where NPs in the leachates were quantitatively indistinguishable from those in the precipitation (t-test, $p > 0.05$). This result was more frequently observed for the slanted exposures (**Figure 2**) and was primarily due to relatively high background concentrations with respect to the low quantities of released NPs. In agreement with Azimzada et al. (2020), while no or low release appeared to occur during specific weathering conditions, such as a lack of precipitation (**Supplementary Figure S4**), background concentrations were also highly episodic. Given that the errors were cumulative, detection of NP release was only significant for cases where release was high, and background was low (**Figure 2**). This implies that the measured release quantities are minimum values only, since low release quantities can easily be masked by pre-existing high background concentrations of the Ti containing NPs.

In addition to characterizing the NPs by SP-ICP-MS, Ti in the 0.45-μm filtrate was measured using quantitative ICP-MS, following acidification and heating of the samples. The concentration of NPs determined by integration of the SP-ICP-MS peaks corresponded to about 10–30% of the values determined based on the digested filtrates of the paint and stain leachates. While the remaining fraction of Ti could be dissolved forms or Ti NPs below the instrumental detection limits, it is also important to acknowledge that a fraction of the missing mass balance could be attributed to sorptive losses in the sample introduction system (Azimzada et al., 2017; Fréchette-Viens et al., 2017; Hadioui et al., 2019) and losses due to incomplete ionization (Goodall et al., 1993; Meermann and Nischwitz, 2018; Hadioui et al., 2019) (recall that SP-ICP-MS is necessarily performed on non-acidified samples).

The size distributions of the NPs released from the painted (**Supplementary Figure S5B**) and stained (**Supplementary Figure S5C**) surfaces were similar to NPs found in the natural precipitation (**Supplementary Figure S5A**). For example, paint-released NPs were mostly <60 nm, with a size range from

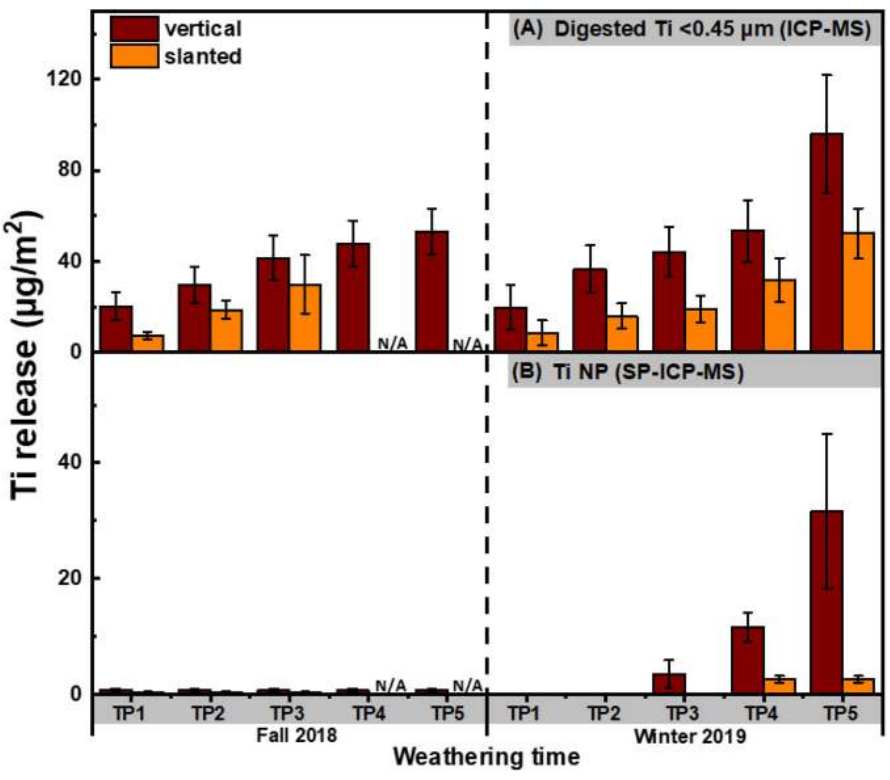

FIGURE 4 | Cumulative concentrations of sub-0.45-μm Ti determined by **(A)** ICP-MS on acidified samples and **(B)** SP-ICP-MS, obtained by integration of the NP peaks. Ti was measured following its release from the **stained** surfaces in vertical and slanted exposure modes (N = 4 for each condition). Release was normalized by the surface area of the painted panels that were subject to weathering and corrected for the pre-existing natural background in the precipitation. Measurements were performed using a magnetic sector ICP-MS. N/A denotes two samples that were lost.

15–120 nm in agreement with our previous results (Azimzada et al., 2020). Generally, they had smaller sizes than those originally found in the liquid paint (**Supplementary Figure S3A**), indicating that there was some agglomeration in the original paint mixture. In contrast, NPs released from the stained surfaces ranged from 15–100 nm with a size distribution (**Supplementary Figure S5C**) that was similar to the original particles in the stain (**Supplementary Figure S3B**).

Role of Exposure Mode (Vertical or Slanted), Season (Fall or Winter) and Coating Type (Paint or Stain)

Generally speaking, less TiO_2 NP release was observed for the slanted exposures where precipitation was not allowed to remain in contact with the panels (**Figures 3**, **4**). Furthermore, NP release from the vertical painted surfaces was still several times less than that observed in Azimzada et al. (2020) and others (Kägi et al., 2008; Olabarrieta et al., 2012; Zuin et al., 2014; Zhang et al., 2017), where much longer weathering times or accelerated weathering conditions were used in a similar experimental design. The results show that NPs are more likely to be leached from surfaces that have a prolonged exposure to precipitation.

While comparable NP release was observed for the painted surfaces that were weathered in fall or winter; for the stain, NP release was clearly greater in the winter (t-test, $p < 0.05$) (**Figures 3B**, **4B**). It is also notable that most NP release did not occur in the initial stages of the exposure (<3 μg-Ti m^{-2} over the first 4,5 weeks, corresponding to timepoints 1 and 2), but rather during the final 6,7 weeks (i.e., last three timepoints) of the weathering period. This observation could be attributed to two possible explanations: (i) an initial weathering period rendered

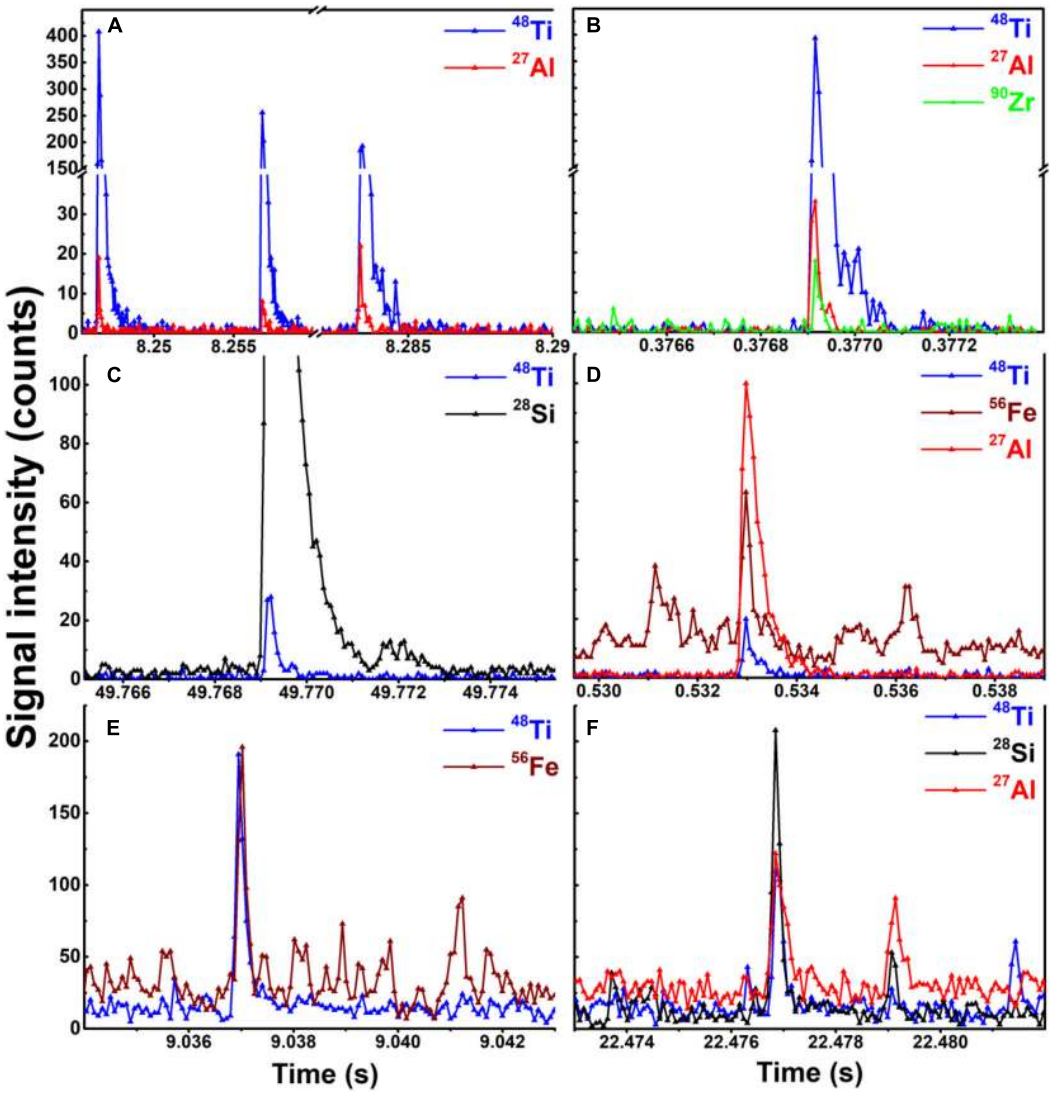

FIGURE 5 | Examples of SP-ICP-TOF-MS raw peak data corresponding to Ti-containing NPs detected in the different matrices. Association of Ti with **(A)** Al or with **(B)** Al and Zr in the liquid paint. Association of Ti with **(C)** Si or with **(D)** Fe and Al in the liquid stain. Association of Ti with **(E)** Fe and **(F)** Si and Al in Montreal rain.

the samples more vulnerable to NP release in the subsequent weeks, or (ii) the samples were exposed to conditions that were more conducive to NP release during the final weeks of the fall and winter exposure period (Azimzada et al., 2020). Indeed, weather data (**Supplementary Figure S4**) reveals that more numerous incidents of precipitation, slushy snow and freeze-thaw conditions (about 20 rainy/snowy days with temperatures fluctuating between +10°C and −10°C) were observed near the end of fall and winter seasons. Irrespective of the NP release trend, Ti NPs in the leachate consistently increased over time in both the fall and winter (**Figures 3A**, **4A**).

NP release from painted surfaces was fairly small, eventually surpassing 10 μg-Ti m^{-2} by the end of the 11-week fall weathering experiment and remaining slightly below 10 μg-Ti m^{-2} during the winter exposure (**Figure 3B**). Release from stained surfaces was very low (<1 μg-Ti m^{-2}) and neither increased throughout fall, nor during the first 4 weeks of the winter exposure (**Figure 4B**). During the spring snowmelt period, however, the quantities of NPs released from the stain greatly surpassed those released from paint, eventually exceeding 30 μg-Ti m^{-2}. While the absolute quantities (mass normalized by surface area) released from painted and stained surfaces were generally on the same order of magnitude, when given as a proportion of the total Ti NPs in the coatings, Ti release from the stained surfaces (max release about 6%) was several orders of magnitude greater than that released from painted surfaces (max release about 5×10^{-5}%). This result might be related to the size distribution in the original coating, as smaller particles are thought to be more easily released from the matrix due to weathering/crack formation, etc. (Bossa et al., 2017) which could also help explain the similarity of the release histograms observed in **Supplementary Figure S5**. Overall, it is clear that NP leaching is strongly influenced by the chemistry of the coating and that some nano-enhanced surfaces (e.g., stained surfaces) are much more vulnerable to NP release than others.

Distinguishing the Engineered NPs From Background NPs in the Precipitation Using SP-ICP-TOF-MS

SP-ICP-TOF-MS measurements on the NPs in the diluted paint and stain showed that in addition to Ti-containing NPs, several other particle types were observed including those containing Fe, Al, Zr, Ce, and Si. In both paints and stains, Ce (i.e., CeO_2) (Piccinno et al., 2012; Clar et al., 2018; Scifo et al., 2018) and Si (i.e., SiO_2) (Zhou et al., 2002; Mizutani et al., 2006; Al-Kattan et al., 2015) are known to impart thermal/mechanical resistance and weathering durability (e.g., against UV) to the coatings, while Al, Fe and Zr NPs could be purposefully added to improve coating properties (Piccinno et al., 2012) or could simply be present as impurities from the manufacturing process. Clear differences were observed when comparing the nature of the particles in the paint (**Supplementary Figure S6**) to those in the stain (**Supplementary Figure S7**). Peak co-incidences indicated that the Ti-containing NPs in the liquid paint (**Figures 5A,B**) were often associated with Al (<20% of TiO_2 NPs) and rarely with Zr (<1% of TiO_2 NPs) (**Figure 6A**). Nonetheless, over 70% of the particles had Ti/Al or Ti/Zr mass ratios above 10, when calculated on a particle by particle basis (**Figures 7A,B**). Three alternative explanations are proposed to explain these high ratios in the paint: (i) traces of Al or Zr, whether in dissolved or small NP forms, were bound to Ti-containing NPs or their agglomerates; (ii) these metals (or their oxides) were used as coatings on Ti-containing NPs (Loosli et al., 2019); or (iii) there were impurities in the Ti-containing NPs. In contrast to measurements on the liquid paint, no Al and almost no Zr were detected in the Ti-containing NPs in the paint leachate (**Figure 6B**), even though high amounts of dissolved Al were observed as compared to the controls (**Supplementary Figure S8**). The absence of Al in the Ti NPs found in the leachate suggests that during the weathering of the painted surface, TiO_2 NPs were separated from an Al-containing matrix (hypothesis i), resulting in increased dissolved Al concentrations. The low detection of Zr in the leachate could simply be explained by its low concentration (relative to instrument detection limits).

In the liquid stain, Ti-containing NPs were often associated with Fe (∼7%) and Si (∼8%) and less often with Al (∼3%, **Figures 5C,D**). This result is not direct evidence that Fe, Si, or

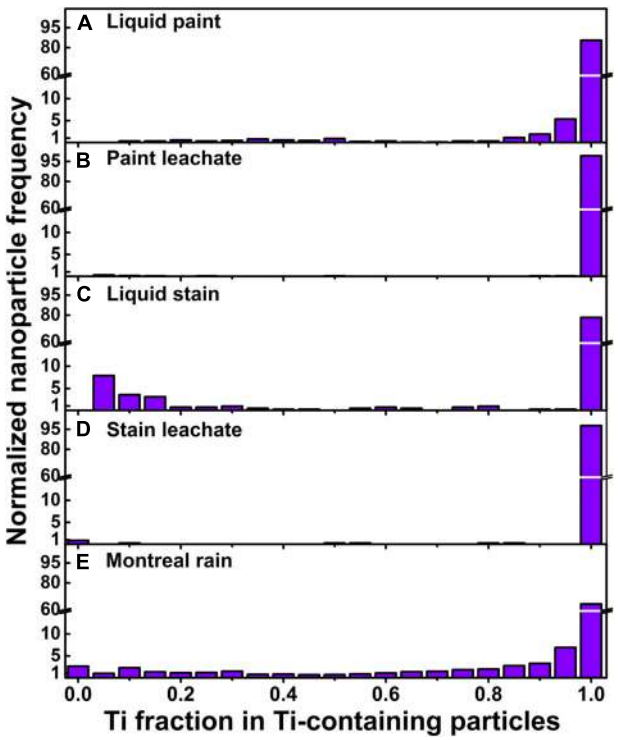

FIGURE 6 | Elemental fractions of Ti in Ti-containing NPs for **(A)** liquid paint (diluted in Milli-Q water), **(B)** paint leachate, **(C)** liquid stain (diluted in Milli-Q water), **(D)** stain leachate, and **(E)** Montreal rainwater. Measurements were performed using a SP-ICP-TOF-MS. Under the described conditions, a Ti fraction of 1 implies that the NP is primarily composed of Ti (or TiO_2, i.e., single metal), whereas fractions < 1 indicate the presence of additional metals within the NP or agglomerate. Paint and stain leachates were collected during accelerated weathering experiments of the coated panels in Milli-Q water.

Al co-occurred with the Ti of a given NP, since Ti-containing NPs could have simply been associated with particles such as aluminosilicates within heteroagglomerates. Indeed, given that the Ti fraction was often below 0.2 (**Figure 6C**), it is possible that small TiO_2 NPs (often <50 nm, **Supplementary Figure S3B**) were associated with larger Fe and Si based particles in the liquid stain (**Figures 7C,D**). This hypothesis of heteroagglomeration was reinforced by the relatively high particle numbers that were found for the Fe and Si NPs, i.e., 1 Ti NP was detected per 25 Fe NPs/10 Si NPs. Given that the vast majority of Ti NPs in the leachate (>95% of NPs) were not associated with any other metals (including Fe or Si) (**Figure 6D**), the results are another indication that the nature of the Ti NPs within the painted or stained surfaces is different from that found in the leachate, following the weathering process. The observation that Ti NPs in the leachate are primarily "pure" particles is important from the perspective of risk analysis.

SP-ICP-MS measurements showed a significant presence of Ti-containing NPs in the rain and snow, which are thought to result from both anthropogenic activities and natural processes (Hochella et al., 2019; Rahim et al., 2019). Generally, engineered NPs are assumed to contain a single element with trace impurities (if any) (Praetorius et al., 2017), whereas NPs of natural origin are believed to more often contain multiple elements. Using elemental purity as an indicator for the origin of the NPs, up to 50% of the Ti-containing NPs in Montreal rain/snowmelt could be classified as engineered NPs (with >99% purity), while the rest had multi-element identities (**Figure 6E**). In the multi-element particles, Ti typically co-occurred with Fe and less often with Al and Si (**Figures 5E,F**, **7E,F**), further supporting the hypothesis

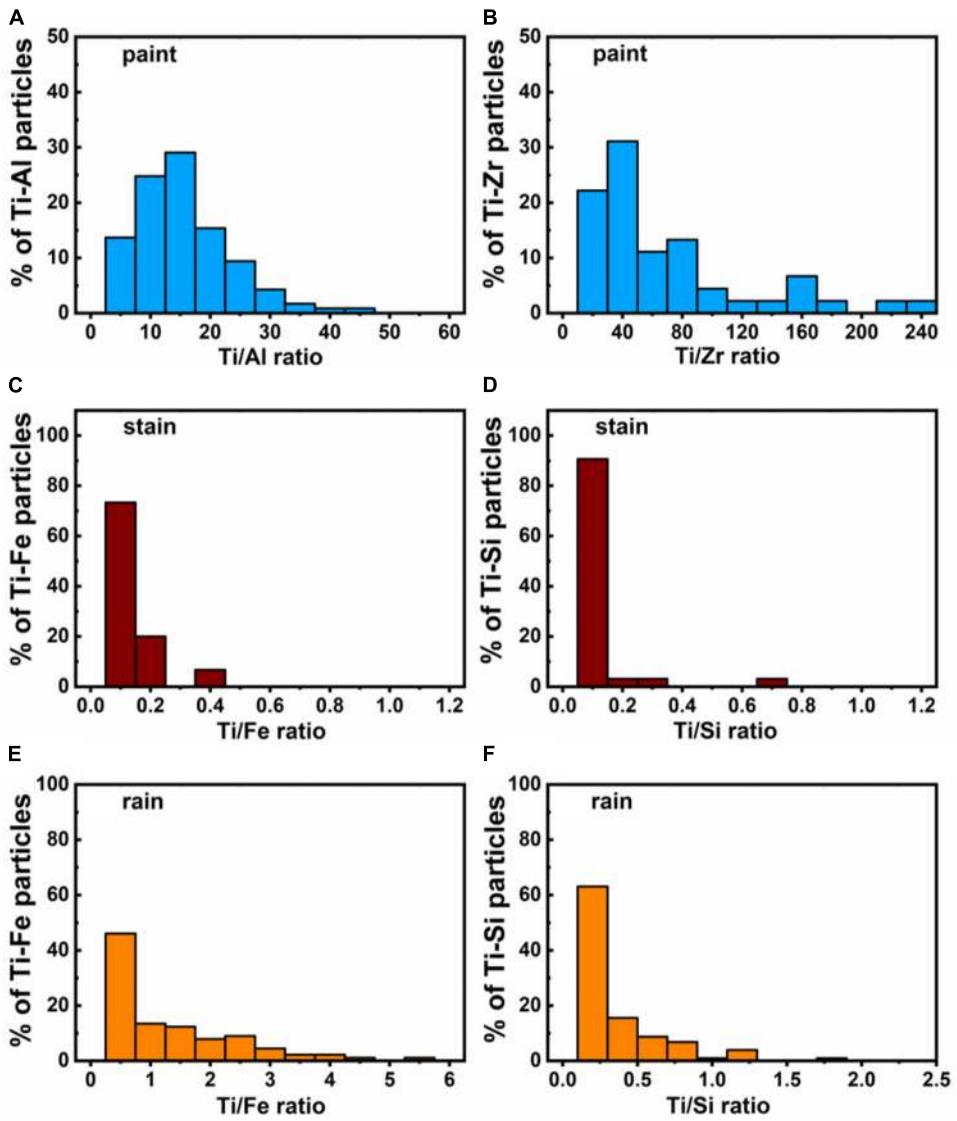

FIGURE 7 | Elemental mass ratios measured on individual particles for major associations of the Ti in **(A,B)** liquid paint, **(C,D)** liquid stain and **(E,F)** Montreal rain samples. Measurements were performed using a SP-ICP-TOF-MS.

that they were naturally occurring particulates (Hochella et al., 2008; Plathe et al., 2013). Nonetheless, the ratio of single element particles should be used carefully when distinguishing NP source since it will vary geographically and temporally, as a function of urban, industrial or natural setting of the location and/or episodic events. While multi-element Ti particles predominate in nature, it is possible for TiO_2 nanoparticles to occur naturally. The environmental release of anthropogenic TiO_2, including those from the paints and stains, will nevertheless increase the overall proportion of Ti in the Ti-containing particles (**Figure 6**), providing an indication of particle source.

Environmental Implications

TiO_2 NPs were leached out of both painted and stained surfaces under natural weathering conditions. For the products tested here, absolute release quantities were comparable (i.e., within one order of magnitude), although this was mainly because there were initially far more NPs in the paint and far greater release by the stain. NP release dynamics were largely driven by the nature of contact with the precipitation. For instance, for scenarios where the panels were in extended contact with sitting water or snow (e.g., on a deck), stronger NP release was observed as compared to the weathering of surfaces where precipitation was not allowed to accumulate (e.g., outdoor facades). While the weathering experiments were performed under realistic environmental scenarios, losses of the NP due to agglomeration (Azimzada et al., 2020; Farner et al., 2020) and a potential underestimation of the measured NP concentrations (Azimzada et al., 2017; Hadioui et al., 2019) implies that the actual release rates could be higher in environmental systems. On the other hand, the recovered (measured) NP concentrations are likely to represent the most mobile and bioavailable fraction that is likely to be of highest environmental relevance.

It is of note that the individual NP appeared to be associated with multiple elements in the pure stain and paint, whereas after weathering of the dried compounds from the surfaces, particles were more elementally pure, suggesting dissociation from a complex matrix. The results also indicated that the particles in the leachates were smaller than NPs detected in the rain, which often had multi-element identities, and thus, larger sizes than those estimated using analysis with a single isotope (i.e., SP-ICP-MS). This implies that, in addition to NPs, other compounds, including potentially toxic ones, are being released during the degradation of these nano-enhanced surfaces. Finally, while anthropogenic NPs already appear to have a significant presence in precipitation, NP release from consumer products, such as paints and stain, will only contribute further to their presence in the environment.

DATA AVAILABILITY STATEMENT

The raw data supporting the conclusions of this article will be made available by the authors, without undue reservation, to any qualified researcher.

AUTHOR CONTRIBUTIONS

KW, JF, NT, and AA conceived the study and designed the experimental plan. AA, JF, IJ, and CL-K prepared the weathering setups, collected the samples and prepared them for single particle and total metal analysis. AA and MH conducted SP-ICP-MS analysis. AA and PS conducted SP-ICP-TOF-MS analysis. AA, MH, and PS performed the SP-ICP(-TOF)-MS data treatment. AA organized all data and performed statistics. AA and KW wrote the manuscript, with complementary input from other authors. All authors contributed to the article and approved the submitted version.

FUNDING

This research was supported by the Natural Sciences and Engineering Research Council of Canada (NSERC), Environment and Climate Change Canada, a McGill Engineering Doctoral Award (MEDA), Pollution in Urban Environments (PURE CREATE) and an EcotoQ Excellence Scholarship.

ACKNOWLEDGMENTS

We thank Prof. Ghoshal (McGill University) for providing access to a film applicator.

SUPPLEMENTARY MATERIAL

The Supplementary Material for this article can be found online at: https://www.frontiersin.org/articles/10.3389/fenvs.2020.00091/full#supplementary-material

REFERENCES

Al-Kattan, A., Wichser, A., Vonbank, R., Brunner, S., Ulrich, A., Zuin, S., et al. (2013). Release of TiO2 from paints containing pigment-TiO2 or nano-TiO2 by weathering. *Environ. Sci. Process. Impacts* 15, 2186–2193.

Al-Kattan, A., Wichser, A., Vonbank, R., Brunner, S., Ulrich, A., Zuin, S., et al. (2015). Characterization of materials released into water from paint containing nano-SiO2. *Chemosphere* 119, 1314–1321. doi: 10.1016/j.chemosphere.2014.02.005

Al-Kattan, A., Wichser, A., Zuin, S., Arroyo, Y., Golanski, L., Ulrich, A., et al. (2014). Behavior of TiO2 released from nano-TiO2-containing paint and comparison to pristine nano-TiO2. *Environ. Sci. Technol.* 48, 6710–6718. doi: 10.1021/es5006219

Auffan, M., Rose, J., Wiesner, M. R., and Bottero, J.-Y. (2009). Chemical stability of metallic nanoparticles: a parameter controlling their potential cellular toxicity in vitro. *Environ. Pollut.* 157, 1127–1133. doi: 10.1016/j.envpol.2008.10.002

Azimzada, A., Farner, J. M., Hadioui, M., Liu-Kang, C., Jreije, I., Tufenkji, N., et al. (2020). Release of TiO2 nanoparticles from painted surfaces in cold climates: characterization using a high sensitivity single-particle ICP-MS. *Environ. Sci. Nano* 7, 139–148. doi: 10.1039/c9en00951e

Azimzada, A., Tufenkji, N., and Wilkinson, K. J. (2017). Transformations of silver nanoparticles in wastewater effluents: links to Ag bioavailability. *Environ. Sci. Nano* 4, 1339–1349. doi: 10.1039/c7en00093f

Bossa, N., Chaurand, P., Levard, C., Borschneck, D., Miche, H., Vicente, J., et al. (2017). Environmental exposure to TiO2 nanomaterials incorporated in building material. *Environ. Pollut.* 220, 1160–1170. doi: 10.1016/j.envpol.2016.11.019

Clar, J. G., Platten, W. E. III, Baumann, E., Remsen, A., Harmon, S. M., Rodgers, K., et al. (2019). Release and transformation of ZnO nanoparticles used in outdoor surface coatings for UV protection. *Sci. Total Environ.* 670, 78–86. doi: 10.1016/j.scitotenv.2019.03.189

Clar, J. G., Platten, W. E. III, Baumann, E. J. Jr., Remsen, A., Harmon, S. M., Bennett-Stamper, C. L., et al. (2018). Dermal transfer and environmental release of CeO2 nanoparticles used as UV inhibitors on outdoor surfaces: implications for human and environmental health. *Sci. Total Environ.* 613, 714–723. doi: 10.1016/j.scitotenv.2017.09.050

Coll, C., Notter, D., Gottschalk, F., Sun, T., Som, C., and Nowack, B. (2016). Probabilistic environmental risk assessment of five nanomaterials (nano-TiO2, nano-Ag, nano-ZnO, CNT, and fullerenes). *Nanotoxicology* 10, 436–444. doi: 10.3109/17435390.2015.1073812

De la Calle, I., Menta, M., and Seby, F. (2016). Current trends and challenges in sample preparation for metallic nanoparticles analysis in daily products and environmental samples: a review. *Spectrochim. Acta Part B At. Spectrosc.* 125, 66–96. doi: 10.1016/j.sab.2016.09.007

Degueldre, C., Favarger, P.-Y., and Wold, S. (2006). Gold colloid analysis by inductively coupled plasma-mass spectrometry in a single particle mode. *Anal. Chim. Acta* 555, 263–268. doi: 10.1016/j.aca.2005.09.021

del Real, A. E. P., Castillo-Michel, H., Kaegi, R., Larue, C., de Nolf, W., Reyes-Herrera, J., et al. (2018). Searching for relevant criteria to distinguish natural vs. anthropogenic TiO2 nanoparticles in soils. *Environ. Sci. Nano* 5, 2853–2863. doi: 10.1039/c8en00386f

Farner, J. M., Cheong, R. S., Mahé, E., Anand, H., and Tufenkji, N. (2019). Comparing TiO2 nanoparticle formulations: stability and photoreactivity are key factors in acute toxicity to *Daphnia magna*. *Environ. Sci. Nano* 6, 2532–2543. doi: 10.1039/c9en00666d

Farner, J. M., De Tommaso, J., Mantel, H., Cheong, R. S., and Tufenkji, N. (2020). Effect of freeze/thaw on aggregation and transport of nano-TiO2 in saturated porous media. *Environ. Sci. Nano* 7, 1781–1793.

Fréchette-Viens, L., Hadioui, M., and Wilkinson, K. J. (2017). Practical limitations of single particle ICP-MS in the determination of nanoparticle size distributions and dissolution: case of rare earth oxides. *Talanta* 163, 121–126. doi: 10.1016/j.talanta.2016.10.093

Fréchette-Viens, L., Hadioui, M., and Wilkinson, K. J. (2019). Quantification of ZnO nanoparticles and other Zn containing colloids in natural waters using a high sensitivity single particle ICP-MS. *Talanta* 200, 156–162. doi: 10.1016/j.talanta.2019.03.041

Gondikas, A., von der Kammer, F., Kaegi, R., Borovinskaya, O., Neubauer, E., Navratilova, J., et al. (2018). Where is the nano? Analytical approaches for the detection and quantification of TiO2 engineered nanoparticles in surface waters. *Environ. Sci. Nano* 5, 313–326. doi: 10.1039/c7en00952f

Gondikas, A. P., Kammer, F. V. D., Reed, R. B., Wagner, S., Ranville, J. F., and Hofmann, T. (2014). Release of TiO2 nanoparticles from sunscreens into surface waters: a one-year survey at the old Danube recreational Lake. *Environ. Sci. Technol.* 48, 5415–5422. doi: 10.1021/es405596y

Goodall, P., Foulkes, M. E., and Ebdon, L. (1993). Slurry nebulization inductively coupled plasma spectrometry-the fundamental parameters discussed. *Spectrochim. Acta Part B At. Spectrosc.* 48, 1563–1577. doi: 10.1016/0584-8547(93)80143-i

Hadioui, M., Knapp, G. V., Azimzada, A., Jreije, I., Frechette-Viens, L., and Wilkinson, K. J. (2019). Lowering the size detection limits of Ag and TiO2 nanoparticles by Single Particle ICP-MS. *Anal. Chem.* 91, 13275–13284. doi: 10.1021/acs.analchem.9b04007

Hendriks, L., Gundlach-Graham, A., and Günther, D. (2018). Analysis of inorganic nanoparticles by single-particle inductively coupled plasma time-of-flight mass spectrometry. *Chim. Int. J. Chem.* 72, 221–226. doi: 10.2533/chimia.2018.221

Hendriks, L., Gundlach-Graham, A., Hattendorf, B., and Günther, D. (2017). Characterization of a new ICP-TOFMS instrument with continuous and discrete introduction of solutions. *J. Anal. At. Spectrom.* 32, 548–561. doi: 10.1039/c6ja00400h

Hincapié, I., Caballero-Guzman, A., Hiltbrunner, D., and Nowack, B. (2015). Use of engineered nanomaterials in the construction industry with specific emphasis on paints and their flows in construction and demolition waste in Switzerland. *Waste Manag.* 43, 398–406. doi: 10.1016/j.wasman.2015.07.004

Hischier, R., Nowack, B., Gottschalk, F., Hincapie, I., Steinfeldt, M., and Som, C. (2015). Life cycle assessment of façade coating systems containing manufactured nanomaterials. *J. Nanopart. Res.* 17:68.

Hochella, M. F., Lower, S. K., Maurice, P. A., Penn, R. L., Sahai, N., Sparks, D. L., et al. (2008). Nanominerals, mineral nanoparticles, and earth systems. *Science* 319, 1631–1635. doi: 10.1126/science.1141134

Hochella, M. F., Mogk, D. W., Ranville, J., Allen, I. C., Luther, G. W., Marr, L. C., et al. (2019). Natural, incidental, and engineered nanomaterials and their impacts on the Earth system. *Science* 363:eaau8299. doi: 10.1126/science.aau8299

Kaegi, R., Englert, A., Gondikas, A., Sinnet, B., von der Kammer, F., and Burkhardt, M. (2017). Release of TiO2–(Nano) particles from construction and demolition landfills. *Nanoimpact* 8, 73–79. doi: 10.1016/j.impact.2017.07.004

Kaegi, R., Sinnet, B., Zuleeg, S., Hagendorfer, H., Mueller, E., Vonbank, R., et al. (2010). Release of silver nanoparticles from outdoor facades. *Environ. Pollut.* 158, 2900–2905. doi: 10.1016/j.envpol.2010.06.009

Kägi, R., Ulrich, A., Sinnet, B., Vonbank, R., Wichser, A., Zuleeg, S., et al. (2008). Synthetic TiO2 nanoparticle emission from exterior facades into the aquatic environment. *Environ. Pollut.* 156, 233–239. doi: 10.1016/j.envpol.2008.08.004

Laborda, F., Gimenez-Ingalaturre, A. C., Bolea, E., and Castillo, J. R. (2019). Single particle inductively coupled plasma mass spectrometry as screening tool for detection of particles. *Spectrochim. Acta Part B At. Spectrosc.* 159:105654.

Lee, S., Bi, X., Reed, R. B., Ranville, J. F., Herckes, P., and Westerhoff, P. (2014). Nanoparticle size detection limits by single particle ICP-MS for 40 elements. *Environ. Sci. Technol.* 48, 10291–10300. doi: 10.1021/es502422v

Liu, S., Zeng, P., Li, X., Thuyet, D. Q., and Fan, W. (2019). Effect of chronic toxicity of the crystalline forms of TiO2 nanoparticles on the physiological parameters of *Daphnia magna* with a focus on index correlation analysis. *Ecotoxicol. Environ. Saf.* 181, 292–300. doi: 10.1016/j.ecoenv.2019.06.014

Loosli, F., Wang, J., Rothenberg, S., Bizimis, M., Winkler, C., Borovinskaya, O., et al. (2019). Sewage spills are a major source of titanium dioxide engineered (nano)-particle release into the environment. *Environ. Sci. Nano* 6, 763–777. doi: 10.1039/c8en01376d

Meermann, B., and Nischwitz, V. (2018). ICP-MS for the analysis at the nanoscale–a tutorial review. *J. Anal. At. Spectrom.* 33, 1432–1468. doi: 10.1039/c8ja00037a

Mitrano, D. M., Motellier, S., Clavaguera, S., and Nowack, B. (2015). Review of nanomaterial aging and transformations through the life cycle of nano-enhanced products. *Environ. Int.* 77, 132–147. doi: 10.1016/j.envint.2015.01.013

Mizutani, T., Arai, K., Miyamoto, M., and Kimura, Y. (2006). Application of silica-containing nano-composite emulsion to wall paint: a new environmentally safe paint of high performance. *Prog. Organ. Coat.* 55, 276–283. doi: 10.1016/j.porgcoat.2005.12.001

Montaño, M. D., Olesik, J. W., Barber, A. G., Challis, K., and Ranville, J. F. (2016). Single particle ICP-MS: advances toward routine analysis of nanomaterials. *Anal. Bioanal. Chem.* 408, 5053–5074. doi: 10.1007/s00216-016-9676-8

Mozhayeva, D., and Engelhard, C. (2020). A critical review of single particle inductively coupled plasma mass spectrometry–A step towards an ideal method for nanomaterial characterization. *J. Anal. At. Spectrom.* doi: 10.1039/C9JA00206E

Nowack, B., Ranville, J. F., Diamond, S., Gallego-Urrea, J. A., Metcalfe, C., Rose, J., et al. (2012). Potential scenarios for nanomaterial release and subsequent alteration in the environment. *Environ. Toxicol. Chem.* 31, 50–59. doi: 10.1002/etc.726

Olabarrieta, J., Zorita, S., Peña, I., Rioja, N., Monzón, O., Benguria, P., et al. (2012). Aging of photocatalytic coatings under a water flow: long run performance and TiO2 nanoparticles release. *Appl. Catal. B Environ.* 123, 182–192. doi: 10.1016/j.apcatb.2012.04.027

Pace, H. E., Rogers, N. J., Jarolimek, C., Coleman, V. A., Higgins, C. P., and Ranville, J. F. (2011). Determining transport efficiency for the purpose of counting and sizing nanoparticles via single particle inductively coupled plasma mass spectrometry. *Anal. Chem.* 83, 9361–9369. doi: 10.1021/ac201952t

Piccinno, F., Gottschalk, F., Seeger, S., and Nowack, B. (2012). Industrial production quantities and uses of ten engineered nanomaterials in Europe and the world. *J. Nanopart. Res.* 14:1109.

Plathe, K. L., Von Der Kammer, F., Hassellöv, M., Moore, J. N., Murayama, M., Hofmann, T., et al. (2013). The role of nanominerals and mineral nanoparticles in the transport of toxic trace metals: field-flow fractionation and analytical TEM analyses after nanoparticle isolation and density separation. *Geochim. Cosmochim. Acta* 102, 213–225. doi: 10.1016/j.gca.2012.10.029

Praetorius, A., Gundlach-Graham, A., Goldberg, E., Fabienke, W., Navratilova, J., Gondikas, A., et al. (2017). Single-particle multi-element fingerprinting (spMEF) using inductively-coupled plasma time-of-flight mass spectrometry (ICP-TOFMS) to identify engineered nanoparticles against the elevated natural background in soils. *Environ. Sci. Nano* 4, 307–314. doi: 10.1039/c6en00455e

Rahim, M. F., Pal, D., and Ariya, P. A. (2019). Physicochemical studies of aerosols at Montreal Trudeau Airport: the importance of airborne nanoparticles containing metal contaminants. *Environ. Pollut.* 246, 734–744. doi: 10.1016/j.envpol.2018.12.050

Robichaud, C. O., Uyar, A. E., Darby, M. R., Zucker, L. G., and Wiesner, M. R. (2009). Estimates of upper bounds and trends in nano-TiO2 production as a basis for exposure assessment. *Environ. Sci. Technol.* 43, 4227–4233. doi: 10.1021/es8032549

Scifo, L., Chaurand, P., Bossa, N., Avellan, A., Auffan, M., Masion, A., et al. (2018). Non-linear release dynamics for a CeO2 nanomaterial embedded in a protective wood stain, due to matrix photo-degradation. *Environ. Pollut.* 241, 182–193. doi: 10.1016/j.envpol.2018.05.045

Shaw, P., and Donard, A. (2016). Nano-particle analysis using dwell times between 10 μs and 70 μs with an upper counting limit of greater than 3× 10 7 and a gold nanoparticle detection limit of less than 10 nm diameter. *J. Anal. At. Spectrom.* 31, 1234–1242. doi: 10.1039/c6ja00047a

Simonin, M., Martins, J. M., Le Roux, X., Uzu, G., Calas, A., and Richaume, A. (2017). Toxicity of TiO2 nanoparticles on soil nitrification at environmentally relevant concentrations: lack of classical dose–response relationships. *Nanotoxicology* 11, 247–255. doi: 10.1080/17435390.2017.1290845

Sun, T. Y., Gottschalk, F., Hungerbühler, K., and Nowack, B. (2014). Comprehensive probabilistic modelling of environmental emissions of engineered nanomaterials. *Environ. Pollut.* 185, 69–76. doi: 10.1016/j.envpol.2013.10.004

Tharaud, M., Gondikas, A. P., Benedetti, M. F., von der Kammer, F., Hofmann, T., and Cornelis, G. (2017). TiO2 nanomaterial detection in calcium rich matrices by spICPMS. A matter of resolution and treatment. *J. Anal. At. Spectrom.* 32, 1400–1411. doi: 10.1039/c7ja00060j

Van Broekhuizen, P., van Broekhuizen, F., Cornelissen, R., and Reijnders, L. (2011). Use of nanomaterials in the European construction industry and some occupational health aspects thereof. *J. Nanopart. Res.* 13, 447–462. doi: 10.1007/s11051-010-0195-9

Vance, M. E., Kuiken, T., Vejerano, E. P., McGinnis, S. P., Hochella, M. F. Jr., Rejeski, D., et al. (2015). Nanotechnology in the real world: redeveloping the nanomaterial consumer products inventory. *Beilstein J. Nanotechnol.* 6, 1769–1780. doi: 10.3762/bjnano.6.181

Wagner, S., Gondikas, A., Neubauer, E., Hofmann, T., and von der Kammer, F. (2014). Spot the difference: engineered and natural nanoparticles in the environment—release, behavior, and fate. *Angew. Chem. Int. Ed.* 53, 12398–12419.

Zhang, X., Wang, M., Guo, S., Zhang, Z., and Li, H. (2017). Effects of weathering and rainfall conditions on the release of SiO2, Ag, and TiO2 engineered nanoparticles from paints. *J. Nanopart. Res.* 19:338.

Zhou, S., Wu, L., Sun, J., and Shen, W. (2002). The change of the properties of acrylic-based polyurethane via addition of nano-silica. *Prog. Organ. Coat.* 45, 33–42. doi: 10.1016/s0300-9440(02)00085-1

Zhu, X., Zhou, J., and Cai, Z. (2011). TiO2 nanoparticles in the marine environment: impact on the toxicity of tributyltin to abalone (*Haliotis diversicolor supertexta*) embryos. *Environ. Sci. Technol.* 45, 3753–3758. doi: 10.1021/es103779h

Zuin, S., Gaiani, M., Ferrari, A., and Golanski, L. (2014). Leaching of nanoparticles from experimental water-borne paints under laboratory test conditions. *J. Nanopart. Res.* 16:2185.

Conflict of Interest: PS is an employee of Nu Instruments, United Kingdom.

The remaining authors declare that the research was conducted in the absence of any commercial or financial relationships that could be construed as a potential conflict of interest.